CrystEngComm

COMMUNICATION

View Article Online
View Journal | View Issue

Cite this: *CrystEngComm*, 2018, **20**, 5949

Received 14th May 2018,
Accepted 3rd September 2018

DOI: 10.1039/c8ce00783g

rsc.li/crystengcomm

Pressure-induced structural phase transition in Li_4Ge

Chun-Mei Hao,[a] Yunguo Li,[a] Qiang Zhu,*[b] Xin-Yi Chen,[a] Zhan-Xin Wang[a] and Yan-Ling Li*[a]

The structural, dynamic, elastic, and electronic properties of Li_4Ge were investigated by means of evolutionary crystal structure prediction in conjunction with first-principles calculations. We find that the ground-state Li_4Ge under ambient conditions has a cubic symmetry. Li_4Ge undergoes a structural phase transition at about 2 GPa from the cubic $P2_13$ phase to the $R\bar{3}m$ phase. The dynamic and mechanical stabilities of $P2_13$ and $R\bar{3}m$ were confirmed by phonon and elastic constant calculations. From the calculated elastic constants, we obtained the elastic moduli and discussed their elastic anisotropy effect. Our calculation shows that the $P2_13$ structure is brittle while the $R\bar{3}m$ structure is ductile. The anisotropic properties of $R\bar{3}m$ are more pronounced than those of $P2_13$ at ambient pressure. $P2_13$-Li_4Ge is a narrow band gap semiconductor while the $R\bar{3}m$ phase is a poor metal.

1. Introduction

Clean energy has attracted extensive attention in recent years because of the increasing pressure from nonrenewable resource depletion and environmental pollution. Unfortunately, most clean energy sources, like solar energy, wind energy, and tidal energy, are intermittent and not convenient for direct utilization. Therefore, rechargeable energy storage devices are pivotal components in the clean energy conversion–storage–usage chain to realize their stable and efficient use.[1,2] Lithium-ion batteries (LIBs) as new next-generation batteries just satisfy the demands of advanced portable electronic devices, electric vehicles, and large-scale energy storage. In the search for new anode materials for LIBs, much attention has been paid to the potential application of group IV elements (Si, Ge, and Sn) in compound forms.[3] Compared with silicon and tin, the expensive germanium draws less attention. However, the diffusivity of the lithium-ion (about 400 times) and electronic conductivity (about 10^4 times) in germanium-based materials are greater than those in silicon. Besides, germanium-based batteries at low operating voltage have remarkable mechanical strength and a theoretical capacity of 1600 mA h g^{-1}, about five times greater than tin (990 mA h g^{-1}).[4–6] In addition, Ge electrodes react with Li through the reversible formation of a nanoporous network, permitting a facile stress relaxation, whereas Si electrodes are often heavily fractured.[7] Germanium has also been proposed as a protective coating for SiNW anodes.[8,9] These observations showing the advantages of germanium-based batteries prompt further studies on the Li–Ge system.

To understand the discharge/charge process and improve the performance of Li–Ge batteries, many research studies have been done on Li–Ge binary compounds. Sangster *et al.*[10] reported a binary phase diagram of the Li–Ge system consisting of seven experimentally reported crystalline phases: Li_7Ge_{12}, LiGe, $Li_{11}Ge_6$, Li_9Ge_4, Li_7Ge_2, $Li_{15}Ge_4$, and $Li_{22}Ge_5$. It is worth noting that the $Li_{22}Ge_5$ phase was reformulated as $Li_{17}Ge_4$ in 2001.[11] With the development of technology and ongoing research, new structures were successively reported. Some new Li–Ge compounds (Li_5Ge_2, $Li_{13}Ge_5$, Li_8Ge_3 and $Li_{13}Ge_4$) were found *via* combined random structure searching and atomic species swapping methods.[12] Jung *et al.*[13] proved that during the discharge process, crystalline Ge first reacts to form a mixture of amorphous and crystalline Li_7Ge_3 which was proposed to be stable in the theoretical study of Morris *et al.*[12] Surprisingly, although Li_4Ge (ref. 14–17) has been suggested for many years in experiments and some research studies on stoichiometries around 4 : 1 ($Li_{4.4}Ge$,[12,18–20] $Li_{4.2}Ge$,[21] $Li_{4.10}Ge$,[22] and $Li_{4.25}Ge$ (ref. 22)) have been reported, the structural information and corresponding properties of Li_4Ge have not yet been determined so far. Given that the analogous compounds Li_4Si,[23] Li_4Sn (ref. 24) and K_4Si,[25] and Li_4C (ref. 26) have been reported, it is highly likely that Li_4Ge may exist as

[a] *School of Physics and Electronic Engineering, Jiangsu Normal University, Xuzhou 221116, China. E-mail: ylli@jsnu.edu.cn*
[b] *Department of Physics and Astronomy, University of Nevada Las Vegas, Las Vegas, NV, 89154-4002, USA. E-mail: qiang.zhu@unlv.edu*

well. This motivated us to explore the stable structure and physical properties of Li_4Ge in the present work.

We have systematically investigated the crystal structures of Li_4Ge up to 10 GPa. Firstly, two competing phases ($P2_13$-Li_4Ge and $R\bar{3}m$-Li_4Ge) have been identified with the help of the evolutionary crystal structure prediction as implemented in the USPEX code.[27–29] The dynamic stabilities of the two competing phases were confirmed by calculating the phonon spectra. Secondly, we discussed the elastic and electronic properties of the two Li_4Ge phases. The results obtained here can enrich the Li–Ge phase diagram and may provide an important reference for the application of LIBs in practice. We believe that our study can further stimulate experimental and theoretical studies on alkali metal-IVA compounds.

2. Computational methods

The evolutionary algorithm USPEX[27–29] in combination with the VASP package[30] is capable of predicting the stable structure of a compound under a specific chemical composition. Here, the structure predictions were performed at 0 GPa, 5 GPa, and 10 GPa for Li_4Ge with the constraint that the total number of atoms in the unit cell is up to 20. In the evolutionary structural search, a plane-wave basis set cutoff of 600 eV and a coarse k-point grid were used to perform the Brillouin-zone integrations. The first generation of structures was created randomly with a population size of 120 structures. The succeeding generations were produced by 40% variation operator heredity, 20% lattice mutation, and 20% permutation. Candidate structural relaxation was performed using density functional theory (DFT) within the generalized gradient approximation (GGA)[31] as implemented in the VASP code.[30] The projector augmented wave (PAW) method was used to treat core electrons.[32] The electron configurations $1s^22s^1$ and $3d^{10}4s^24p^2$ are treated as valence states for Li and Ge, respectively. A higher Brillouin-zone sampling of $2\pi \times 0.028$ Å^{-1} and the plane-wave basis set cutoff of 600 eV were used, in order to ensure that the enthalpy calculations were converged within 1 meV per atom. Structural relaxation was stopped when the force generally acting on the atom was found to be less than 0.001 eV Å^{-1}. Phonon spectra calculations were conducted by the finite displacement method as implemented in the PHONOPY code.[33,34] The elastic constants were calculated based on linear response theory.[35] Using the obtained elastic constants C_{ij}, the bulk modulus B and shear modulus G were calculated using the Voigt–Reuss–Hill (VRH) approximation.[36] Young's modulus E and Poisson's ratio v can be calculated by the formulae $E = \frac{9BG}{3B+G}, v = \frac{3B-2G}{2(3B+G)}$.

3. Results and discussion

3.1. Crystal structure

In our crystal structure search, we have found two competing structures (space groups $P2_13$ and $R\bar{3}m$). The corresponding crystallographic information under ambient pressure conditions is listed in Table 1. For the $P2_13$ phase, there are three different Wyckoff sites, Ge (4a), Li1 (12b) and Li2 (4a). Each Ge atom is six-fold coordinated by Li atoms (three Li1 and three Li2), forming irregular octahedra as shown in Fig. 1a. The bond lengths are 2.60 Å for Li1–Ge and 2.66 Å for Li2–Ge, respectively. The octahedra are connected by sharing Li2 atoms located at the vertices. For the hexagonal $R\bar{3}m$ phase, the (distorted) cubic hexahedron (where the length of each side of the distorted cubes is either 2.96 Å or 3.25 Å) consisting of Li-sharing eight-fold $GeLi_8$ is similar to the structure of Li_4Si.[23] Ge atoms occupy the 3b sites. Three-fold coordinated Li1 atoms occupy the crystallographic 6c sites. Li2 atoms located at 6c sites are only connected with one Ge atom. One can notice that a one-dimensional array of Li–Li–Li–Li–Ge runs along the c-axis periodically, as shown in Fig. 1b. In the $GeLi_8$ cube, each Li1 atom is connected with three neighboring Ge atoms from the adjacent cubes, while each Li2 atom is connected with one Ge atom within the cube. Thus, the formation of the structure can be interpreted based on the extended Zintl–Klemm principle where Ge atoms fulfill the "octet" by acquiring two electrons from six Li atoms and two more electrons from other two Li atoms, as expected. At zero pressure, the shortest Li–Li distance in $R\bar{3}m$ is 2.75 Å, which is shorter than 2.83 Å in $P2_13$. The shortest Li–Ge distance (2.70 Å) is longer than 2.66 Å in $R\bar{3}m$. The analogous structures of $R\bar{3}m$ Li_4Ge were proposed for Li_4Si,[23] and Li_4Sn (ref. 24) in two recent computational studies, while the cubic phase is an entirely new structure which has not been reported in the literature to the best of our knowledge.

3.2. Phase transition

In order to determine the stability of the two new Li_4Ge phases, we recalculated the convex hull diagram of Li–Ge under zero temperature and ambient pressure conditions. As shown in Fig. 2, the $Li_{17}Ge_4$, $Li_{15}Ge_4$, Li_8Ge_3, $Li_{13}Ge_5$, Li_7Ge_3, and LiGe phases are all thermodynamically stable with

Table 1 Lattice parameters and atomic positions of Li_4Ge under ambient pressure conditions

Space group	Density (g cm^{-3})	Lattice parameters (Å, deg)	Atomic fractional coordinates
$P2_13$	2.018	$a = b = c = 6.8441$ $\alpha = \beta = \gamma = 90.00$	Li1 12b (0.9355, 0.1249, 0.2968) Li2 4a (0.3127, 0.3127, 0.3127) Ge1 4a (0.9498, 0.9498, 0.9498)
$R\bar{3}m$	2.141	$a = b = 4.5050$ $c = 13.2938$ $\alpha = \beta = 90$ $\gamma = 120$	Li1 6c (0.0000, 0.0000, 0.1132) Li2 6c (0.0000, 0.0000, 0.2997) Ge1 3b (0.0000, 0.0000, 0.5000)

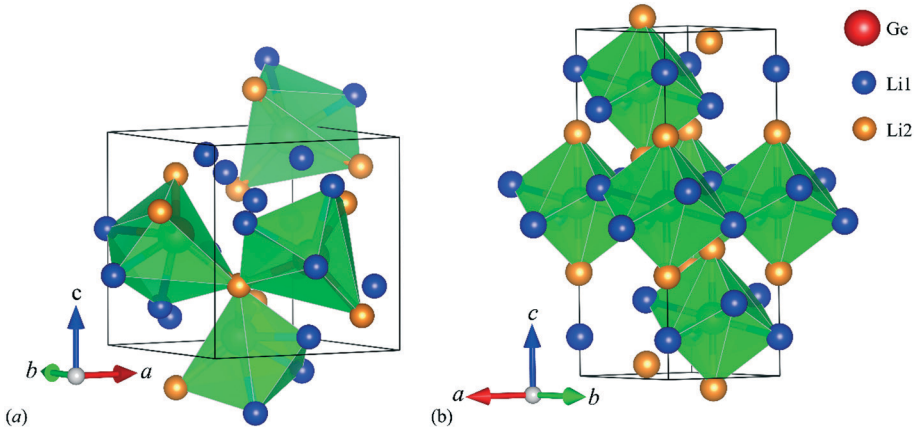

Fig. 1 Crystal structures of Li_4Ge: (a) $P2_13$ and (b) $R\bar{3}m$. Small blue balls, small orange balls, and big red balls represent the Li1 atoms, Li2 atoms and Ge atoms, respectively.

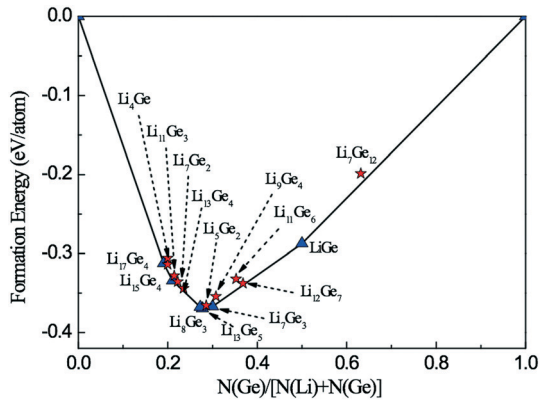

Fig. 2 The calculated convex hull diagram of Li–Ge at 0 K and 0 GPa. The red pentagram indicates the metastable phase, and the blue triangle indicates the stable one.

respect to dissociation into the elements, while Li_4Ge, $Li_{11}Ge_3$, Li_7Ge_2, $Li_{13}Ge_4$, Li_5Ge_2, Li_9Ge_4, $Li_{11}Ge_6$, $Li_{12}Ge_7$ and Li_7Ge_{12} are the metastable ones theoretically. $P2_13$-Li_4Ge is marginally stable. Its decomposition energy to $Li_{17}Ge_4$ and $Li_{15}Ge_4$ is only 6 meV per atom, suggesting that the synthesis of $P2_13$-Li_4Ge is highly possible. On the other hand, the $R\bar{3}m$ phase is slightly less favorable, which is 40 meV per f.u. higher in energy than $P2_13$. However, the relative phase stability with such a small energy difference could be easily switched due to pressure. Therefore, we calculated the enthalpies of the two competing phases as a function of pressure between 0 and 10 GPa. As shown in Fig. 3(a), one can see that under the compression, the cubic $P2_13$ phase transforms into the rhombohedral hexagonal $R\bar{3}m$ phase at 2.0 GPa. Fig. 3(b) shows the volume per chemical formula unit as a function of pressure for the two phases. It is obvious that the phase transition is accompanied by a sudden volume decrease (by 4.13% at 2.0 GPa), indicating that this is a first-order phase transition.

3.3. Dynamic properties

To assessing the dynamic stability of Li_4Ge, we calculated the phonon spectra of $P2_13$-Li_4Ge and $R\bar{3}m$-Li_4Ge. The phonon dispersion curves along the high-symmetry direction and partial phonon density of states (PHDOS) are plotted in Fig. 4(a) and (b) for $P2_13$-Li_4Ge and $R\bar{3}m$-Li_4Ge, respectively.

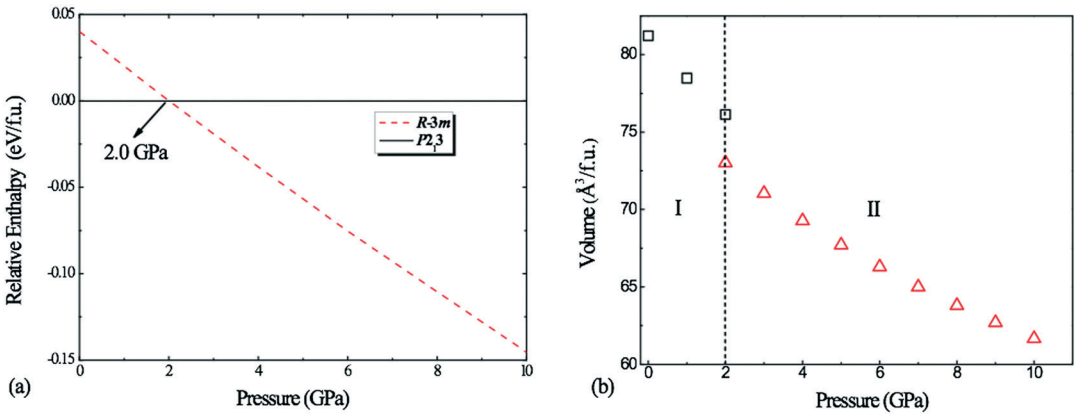

Fig. 3 (a) Enthalpy difference *versus* pressure for the two phases of Li_4Ge. (b) Volume *versus* pressure. Squares and triangles represent I-$P2_13$ and II-$R\bar{3}m$, respectively.

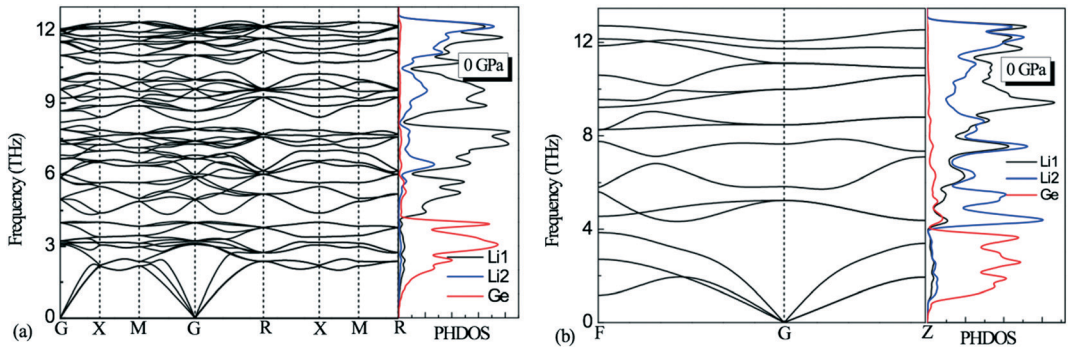

Fig. 4 Phonon dispersion curves and partial atomic phonon density of states (PHDOS) of the phonon spectrum of (a) $P2_13$ Li_4Ge and (b) $R\bar{3}m$ Li_4Ge at 0 GPa.

Table 2 The calculated elastic constants, bulk modulus B (GPa), shear modulus G (GPa), Young's modulus E (GPa), Poisson's ratio ν, and anisotropic index A^U for the $P2_13$ phase at 0 GPa and for the $R\bar{3}m$ phase at 0 GPa and 2 GPa

	P (GPa)	C_{11}	C_{44}	C_{12}	C_{33}	C_{13}	C_{14}	B	G	E	ν	B/G	A^U
$P2_13$	0	44.2	26.2	20.0	—	—	—	28.1	19.2	46.9	0.22	1.46	0.76
$R\bar{3}m$	0	82.3	7.8	9.4	78.1	−3.3	−11.7	27.8	17.3	43.0	0.24	1.60	11.62
$R\bar{3}m$	2	96.0	9.47	12.7	93.8	−2.6	−12.7	33.3	20.8	51.6	0.24	1.60	9.11

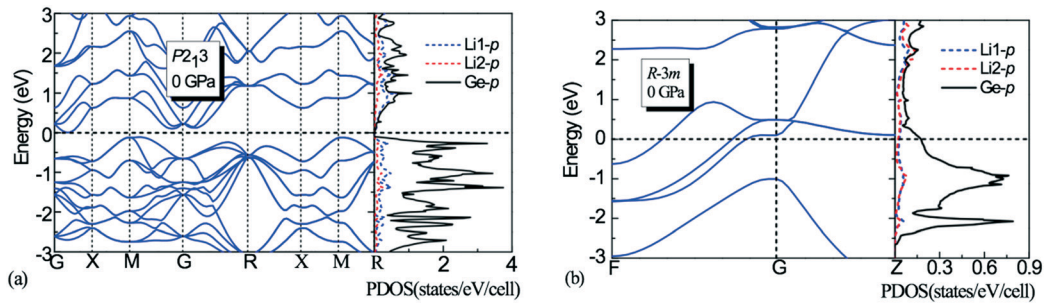

Fig. 5 The electronic band structure and projected density of states (PDOS) at 0 GPa for (a) $P2_13$ Li_4Ge and (b) $R\bar{3}m$ Li_4Ge.

Both phonon dispersion curves show all the positive frequencies in the entire Brillouin zone, indicating the dynamic stability. Thus, they are likely to survive as long as the materials can be synthesized. Although the two structures are different, their maximum optical branch frequencies are very similar (12.408 THz for the $P2_13$ phase and 12.71 THz for the $R\bar{3}m$ phase) at 0 GPa. From the PHDOS, one can conclude that the acoustic branches are mainly attributed to the vibrations from the Ge atoms (below about 4 THz), whereas the higher-frequency optical branches are mainly from Li1 and Li2 atoms, which matches the fact that the Ge atoms are much heavier than the Li atoms.

3.4. Elastic properties

It is well known that the elastic anisotropy of crystals is correlated with the mechanical behavior and the possibility to induce microcracks in the materials.[37] Hence, it is important to discuss the elastic anisotropy so as to understand the mechanical properties of Li_4Ge. In the case of the cubic crystal system, the Born–Huang stability criteria are well known: $C_{44} > 0$, $C_{11}-C_{12} > 0$ and $C_{11} + 2C_{12} > 0$.[38,39] There are six independent elastic constants for the rhombohedral structure (Laue class: $\bar{3}m$), where the required mechanical stability criteria follow the inequalities $C_{11} > |C_{12}|$, $C_{44} > 0$, ${C_{13}}^2 < (C_{11} + C_{12})$ and ${C_{14}}^2 < \frac{1}{2}C_{44}(C_{11}-C_{12}) \equiv C_{44}C_{66}$.[38,39] The calculated elastic constants C_{ij} are presented in Table 2. Clearly, the calculated elastic constants for $P2_13$-Li_4Ge and $R\bar{3}m$-Li_4Ge satisfy the Born–Huang criteria, suggesting that they are mechanically stable as well.

From the calculated elastic constants, one can derive a series of elastic properties such as the bulk modulus B, shear modulus G, Young's modulus E and Poisson's ratio ν based on the VRH approximation (see Table 2). Young's modulus is often used to provide a metric of stiffness of the material. The $P2_13$ phase and $R\bar{3}m$ phase have a Young's modulus of 46.9 GPa and 43.0 GPa at zero pressure,

respectively. At the pressure of 2.0 GPa, the structure of $R\bar{3}m$ gets stiffer. According to Pugh's criterion,[40] if the value of B/G is lower (higher) than 1.75, the material is brittle (ductile). The calculated values of B/G indicated that $P2_13$ and $R\bar{3}m$ are both brittle. The universal anisotropic index A^U is defined as $A^U = 5\frac{G_V}{G_R} + \frac{B_V}{B_R} - 6$.[41] The zero value of A^U indicates the local isotropy. The deviation of this parameter from zero indicates the anisotropy of the crystalline structure. From Table 2, one can conclude that $R\bar{3}m$ is more anisotropic than $P2_13$ at ambient pressure.

3.5. Electronic properties

The calculated electronic band structure along the high symmetry directions in the BZ and the corresponding PDOS at 0 GPa are shown in Fig. 5. Our electronic structure calculations show that the $P2_13$ phase is a semiconductor with a narrow band gap of 0.117 eV. On the other hand, $R\bar{3}m$ Li_4Ge is metallic, in which three bands cross the Fermi level along the *F–G* direction. In both $P2_13$-Li_4Ge and $R\bar{3}m$-Li_4Ge, Ge-p states dominate the whole valence bands while Li-p states have a minor contribution.

4. Conclusions

In summary, two structures were proposed for Li_4Ge by using the evolutionary algorithm structure search. The $P2_13$ phase was found to be stable below 2.0 GPa, while the $R\bar{3}m$ phase is stable above 2.0 GPa. The calculated phonon spectra and elastic constants confirmed their dynamic and mechanical stabilities. Elastic calculations suggest that the $P2_13$ structure is brittle, while the $R\bar{3}m$ structure is ductile. The $R\bar{3}m$ structure is more anisotropic than the $P2_13$ structure at ambient pressure. The electronic structure shows that the $P2_13$ phase is a semiconductor, while the $R\bar{3}m$ phase is a metal. We believe that our findings do not only enrich the phase diagram of the Li–Ge system, but also are beneficial to the design of new anode materials of LIBs.

Conflicts of interest

There are no conflicts to declare.

Acknowledgements

The work at JNSU is supported by the NSFC (Grant No. 11674131) and the Priority Academic Program Development of Jiangsu Higher Education Institutions (PAPD). The work at UNLV is supported by the National Nuclear Security Administration under the Stewardship Science Academic Alliances program through DOE Cooperative Agreement DE-NA0001982. We acknowledge the use of computing resources from XSEDE and High Performance Computing Center at JNSU.

References

1 D. Liu, Z. J. Liu, X. Li, W. Xie, Q. Wang, Q. Liu, Y. Fu and D. He, *Small*, 2017, **13**, 1236–1247.
2 M. Armand and J. M. Tarascon, *Nature*, 2008, **451**, 652–657.
3 A. G. Morachevskii, *Russ. J. Appl. Chem.*, 2017, **89**, 1561–1572.
4 H. Tian, F. Xin, X. Wang, W. He and W. Han, *J. Materiomics*, 2015, **1**, 153–169.
5 C. M. Park, J. H. Kim, H. Kim and H. J. Sohn, *Chem. Soc. Rev.*, 2010, **39**, 3115–3141.
6 C. Y. Chou, H. Kim and G. S. Hwang, *J. Phys. Chem. C*, 2011, **115**, 20018–20026.
7 X. H. Liu, S. Huang, S. T. Picraux, J. Li, T. Zhu and J. Y. Huang, *Nano Lett.*, 2011, **11**, 3991–3997.
8 T. Song, H. Cheng, H. Choi, J. H. Lee, H. Han, D. H. Lee, D. S. Yoo, M. S. Kwon, J. M. Choi, S. G. Doo, H. Chang, J. Xiao, Y. Huang, W. I. Park, Y. C. Chuang, H. Kim, J. A. Rogers and U. Paik, *ACS Nano*, 2012, **6**, 303–309.
9 Y. Yu, C. Yue, S. Sun, W. Lin, H. Su, B. Xu, J. Li, S. Wu, J. Li and J. Kang, *ACS Appl. Mater. Interfaces*, 2014, **6**, 5884–5890.
10 J. Sangster and A. D. J. Pelton, *J. Phase Equilib.*, 1997, **18**, 289–294.
11 G. R. Goward, N. J. Taylor, D. C. S. Souza and L. Nazar, *J. Alloys Compd.*, 2001, **329**, 82–91.
12 A. J. Morris, C. P. Grey and C. J. Pickard, *Phys. Rev. B: Condens. Matter Mater. Phys.*, 2014, **90**, 054111.
13 H. Jung, P. K. Allan, Y. Y. Hu, O. J. Borkiewicz, X. L. Wang, W. Q. Han, L. S. Du, C. J. Pickard, P. J. Chupas, K. W. Chapman, A. J. Morris and C. P. Grey, *Chem. Mater.*, 2015, **27**, 1031–1041.
14 E. M. Pell, *J. Phys. Chem. Solids*, 1957, **3**, 74–76.
15 P. I. Federov and V. A. Molochka, *Izv. Akad. Nauk SSSR, Neorg. Mater.*, 1966, **2**, 1870–1871.
16 A. Grüttner, R. Nesper and H. G. von Schnering, *Acta Crystallogr., Sect. A: Cryst. Phys., Diffr., Theor. Gen. Crystallogr.*, 1981, **37**, C-161.
17 A. Grüttner, *PhD thesis*, University of Stuttgart, 1982.
18 E. L. Gladyshevskii, G. I. Oleksiv and P. I. Kripyakevich, *Sov. Phys. Crystallogr.*, 1964, **9**, 269.
19 E. I. Gladyshevskii, G. I. Oleksiv and P. I. Kripyakevich, *Kristallografiya*, 1964, **9**, 338–341.
20 S. Yoon, C. M. Park and H. J. Sohn, *Electrochem. Solid-State Lett.*, 2008, **11**, A42–A45.
21 R. Nesper, *Prog. Solid State Chem.*, 1990, **20**, 1–45.
22 M. Zeilinger and T. F. Fässler, *Dalton Trans.*, 2014, **43**, 14959–14970.
23 S. T. Zhang, Y. C. Wang, G. C. Yang and Y. M. Ma, *ACS Appl. Mater. Interfaces*, 2016, **8**, 16761–16767.
24 R. Sen and P. Johari, *ACS Appl. Mater. Interfaces*, 2017, **9**, 40197–40206.
25 C. M. Hao, Y. Li, H. M. Huang and Y. L. Li, *J. Chem. Phys.*, 2018, **148**, 204706.
26 Y. Lin, T. A. Strobel and R. E. Cohen, *Phys. Rev. B: Condens. Matter Mater. Phys.*, 2015, **92**, 214106.
27 A. O. Lyakhov, A. R. Oganov, H. T. Stokes and Q. Zhu, *Comput. Phys. Commun.*, 2013, **184**, 1172–1182.
28 A. R. Oganov and C. W. Glass, *J. Chem. Phys.*, 2006, **124**, 244704–244715.

29 A. R. Oganov, A. O. Lyakhov and M. Valle, *Acc. Chem. Res.*, 2011, **44**, 227–237.
30 W. Dong, G. Kresse, J. Furthmüller and J. Hafner, *Phys. Rev. B: Condens. Matter Mater. Phys.*, 1996, **54**, 2157–2166.
31 J. P. Perdew, K. Burke and M. Ernzerhof, *Phys. Rev. Lett.*, 1996, **77**, 3865–3868.
32 P. E. Blöchl, *Phys. Rev. B: Condens. Matter Mater. Phys.*, 1994, **50**, 17953–17979.
33 K. Parlinski, Z. Q. Li and Y. Kawazoe, *Phys. Rev. Lett.*, 1997, **78**, 4063–4066.
34 A. Togo, F. Oba and I. Tanaka, *Phys. Rev. B: Condens. Matter Mater. Phys.*, 2008, **78**, 134106.
35 J. A. Pople, P. W. G. Gill and B. G. Johnson, *Chem. Phys. Lett.*, 1992, **199**, 557–560.
36 R. Hill, *Proc. Phys. Soc., London, Sect. A*, 1952, **65**, 349–354.
37 X. X. Sun, Y. L. Li, G. H. Zhong, H. P. Lü and Z. Zeng, *Phys. Rev. B: Condens. Matter Mater. Phys.*, 2012, **407**, 735–739.
38 F. Mouhat and F. X. Coudert, *Phys. Rev. B: Condens. Matter Mater. Phys.*, 2014, **90**, 224104.
39 M. Born and K. Huang, *Dynamics Theory of Crystal Lattices*, Oxford University Press, Oxford, UK, 1954.
40 S. F. Pugh, *Philos. Mag.*, 1954, **45**, 823–843.
41 S. I. Ranganathan and M. Ostoja-Starzewski, *Phys. Rev. Lett.*, 2008, **101**, 055504.

